Biochimica et Biophysica Acta 1813 (2011) 754–762

Contents lists available at ScienceDirect

Biochimica et Biophysica Acta

journal homepage: www.elsevier.com/locate/bbamcr

Real-time cellular impedance measurements detect Ca^{2+} channel-dependent oscillations of morphology in human H295R adrenoma cells

Athanasios Denelavas [a], Franziska Weibel [a], Michael Prummer [b], Alexander Imbach [a], Roger G. Clerc [a], Christian M. Apfel [a], Cornelia Hertel [a,*]

[a] Metabolic Diseases, F. Hoffmann-La Roche Ltd., Pharma Research and Early Development, Basel, Switzerland
[b] Discovery Technology, F. Hoffmann-La Roche Ltd., Pharma Research and Early Development, Basel, Switzerland

ARTICLE INFO

Article history:
Received 20 August 2010
Received in revised form 7 December 2010
Accepted 13 January 2011
Available online 22 January 2011

Keywords:
Impedance
BayK8644
Ca channel
Exocytosis
Endocytosis
Label-free technology

ABSTRACT

Endocrine cells, such as H295R have been widely used to study secretion of steroid and other hormones. Exocytosis-dependent hormone release is accompanied by an increase in plasma membrane surface area and a decrease in vesicle content. Recovery of vesicles and decrease in plasma membrane area is achieved by endocytotic processes. These changes in the extent of the surface area lead to morphological changes which can be determined by label-free real-time impedance measurements. Exo- and endocytosis have been described to be triggered by activation of L-type Ca^{2+} channels. The present study demonstrates that activation of L-type calcium channels induces prolonged oscillating changes in cellular impedance. The data support the hypothesis that a tight regulation of the intracellular Ca^{2+} concentration is a prerequisite for the observed cellular impedance oscillations. Furthermore evidence is presented for a mechanism in which the oscillations depend on a Ca^{2+}-triggered calmodulin-dependent cascade involving myosin light chain kinase, nonmuscle myosin II and ultimately actin polymerization, a known determinant for cell shape changes and exocytosis in secretory cells. The described assay provides a method to determine continuously prolonged changes in cellular morphology such as exo/endocytosis cycles.

1. Introduction

Adrenocortical H295R cells have been used to investigate angiotensin II (AngII) induced steroid hormone synthesis and secretion [1] as well as peptides [2,3]. Secretion of peptides is mediated by Ca^{2+}-triggered fusion of exocytotic vesicles with the plasma membrane, resulting in an increase in cell surface area. The surplus of plasma membrane has to be tightly balanced by complementary endocytosis to prevent cellular swelling during secretion [4-7]. Exocytosis as well as endocytosis has been described to depend on an increase of the intracellular Ca^{2+} concentration [5], with Ca^{2+} entry through voltage-gated L-type Ca^{2+} channels being one of the mechanisms increasing intracellular Ca^{2+} concentration [6-9]. Several isoforms of the L-type Ca^{2+} channels have been characterized, two of them Cav1.2 and Cav1.3 are widely expressed and also found in endocrine cells, often expressed together in a single cell [10].

Intracellular Ca^{2+} concentration can also be raised after triggering G protein-coupled membrane receptors (GPCRs) that mobilize Ca^{2+} from intracellular storage organelles [6,11]. A subsequent rapid downregulation of intracellular Ca^{2+} concentration is driven by energy-dependent Ca^{2+} pumps that transport Ca^{2+} either across the plasma membrane or back into intracellular Ca^{2+} storage organelles. These oscillations in intracellular Ca^{2+} concentration have been demonstrated using fluorescent Ca^{2+} indicators, such as Fluo-4 [7] and Fura-2 [5]. Increased Ca^{2+} concentrations have been shown to trigger exocytosis by activating calmodulin and subsequently calmodulin-dependent myosin light chain kinase and nonmuscle myosin II [12-16]. Ca^{2+}-dependent exo/endocytosis has been demonstrated to be accompanied by changes in the cell surface morphology that were visualized by scanning ion conductance microscopy observing single cell behavior [17].

Recently label-free real-time technologies have been established which can be used to follow morphological alterations of cells for an extended period of time, without disturbing their environment. Optical sensor based technology detects redistribution of mass close to the plasma membrane, for example due to activation of GPCRs [18] or interaction of ion channels and GPCRs [19]. Cellular impedance-based technology detects changes in the contact area between cells and electrode due to changes in cell morphology, which can be induced by GPCRs [20,21] or tyrosine receptor kinases [22]. In contrast to the optical sensor based method, impedance technology can also be used to follow long term changes in cell growth and cell death [23].

Here we used impedance technology to investigate activation of plasma membrane voltage-dependent L-type Ca^{2+} channels on the morphology of secretory human adrenocarcinoma cells and compared

* Corresponding author at: F. Hoffmann-La Roche Ltd., PMDBCA 70/431, Postfach, CH-4070 Basel, Switzerland. Tel.: +41 61 688 6989; fax: +41 61 688 2438.
E-mail address: cornelia.hertel@roche.com (C. Hertel).

0167-4889/$ – see front matter © 2011 Elsevier B.V. All rights reserved.
doi:10.1016/j.bbamcr.2011.01.016

it to the effect of AngII. AngII induced a rapid decrease followed by an increase in impedance reaching a plateau that stayed constant for several hours. In contrast, opening of L-type Ca^{2+} channels with BayK8644 or FPL64176, two structurally distinct activators of L-type Ca^{2+} channels [24] induced a rapid decrease in impedance followed by impedance oscillations which continued for several hours. Frequency and amplitude of the oscillations are concentration dependent. Membrane depolarization and inhibition of Ca^{2+} channels blocked activation of the signal, while inhibition of processes that decrease the intracellular Ca^{2+} concentration attenuated the oscillations. Oscillations are also prevented by inhibitors of calmodulin-dependent kinase, but interestingly not by inhibitors of protein kinase C. Finally inhibition of nonmuscle myosin II ATPase activity also attenuated the oscillations, indicating that the observed oscillations represent microfilament driven changes in cell shape possibly related to exocytosis/endocytosis cycles.

2. Materials and methods

2.1. Cell culture

H295R (human adrenocortical cells) were grown in DMEM/F12 (Invitrogen) with 2.5% NuSerum (Invitrogen) and 1% IST (BD) in a humidified atmosphere containing 5% CO_2 at 37 °C. For experiments, cells were detached with EDTA solution and seeded at a density of 1.4×10^5 cells/well in 200 μl growth medium.

2.2. RNAi experiments and cell electroporation

H295R cells grown to 80% confluent were placed in each well of an Amaxa 96-well electroporation plate 2×10^5 cells/well. Cells were electroporated with a Nucleofector II Amaxa (Lonza Ltd.) electroporator with the corresponding gene-specific siRNAs (200–500 nM final concentration) in a 96-well nucleofector SF solution (Amaxa VHCA-2002 (Lonza Ltd.), for 24 h for Ca^{2+} channel L-type alpha 1 C subunit (CACNA1C) and 48 h for all other silencing siRNAs. Cells were harvested for RNA extraction and quantification of mRNA levels by qPCR. mRNA levels were compared with those in cells transfected with scrambled siRNA oligonucleotides. All RNAi experiments with sequence-specific siRNAs were tested by qPCR and generated a >60% reduction of the corresponding mRNAs levels.

2.3. RNA extraction and qPCR

qPCR was carried out to determine changes in gene expression. RNA was extracted from H295R cells with QIAshredder and RNeasy kits (QIAGEN). cDNA was synthesized with the Transcriptor First Strand cDNA Synthesis Kit (Roche Diagnostics) and purified with a QIAquick PCR Purification kit (QIAGEN). qPCR assays were performed using a QuantiTect SYBR Green qPCR Kit (QIAGEN) and the Rotor-Gene 6000 (Corbett/Qiagen) with specific DNA primers and glyceraldehyde-3-phosphate dehydrogenase (GAPDH) mRNA as internal reference. Analysis was done by the Δ-Δcycle threshold method to determine fold changes in expression relative to control ($n = 3$). Repeated analysis of variance was applied to statistically compare fold changes across conditions over time (PROC MIXED of SAS v8).

2.4. Life-cell time-lapse microscopy

Cells were seeded in Falcon 96-well plates at 4×10^4 cells/well 18 h prior to experiment. For the Ca^{2+} imaging assay, the manufacturer's protocol was followed using Hanks Balanced Salt Solution + $CaCl_2$ + $MgCl_2$ + 20 mM Hepes (Fluo-4 NW Calcium Assay Kits, F36205, Invitrogen) 30 min prior to the experiment, 1 μM Hoechst stain was added to the cells. Imaging was performed immediately afterwards without further washing. Vehicle treatment consisted of 0.1% DMSO in HBSS, to which 1 μM BayK8644 or 100 nM AngII was added. Spinning-disc confocal fluorescence microscopy of individual wells of a 96-well plate was performed on the high-throughput automated imaging system Opera™ QEHS (PerkinElmer Cellular Technologies, Hamburg, Germany). The nuclear stain and the Ca^{2+} indicator were excited with 1 mW at 405 nm and with 50 μW at 488 nm, respectively. At a single position in each well, a series of 50 images was recorded through a UAPO 20 × NA 0.7 water immersion objective lens (Olympus) and optimized filter sets, with a frame rate of 0.4 s^{-1} and an integration time of 0.4 s and 1.0 s for the DNA channel and the Ca channel, respectively. Time-lapse life-cell microscopy was performed with manual compound addition under ambient conditions. Image registration was started once the sample was in the focal plane of the confocal microscope. After a few (1–3) frames were recorded, compound was added by complete replacement of the HBSS to ensure a homogeneous compound concentration across the whole well.

2.5. Determination of intracellular $Ca2^{+}$ concentration

For the assay, cells were grown overnight in 384-well black clear flat bottom polystyrene plates (Costar) at 37 °C at 5% CO_2. After washing with DMEM, 20 mM Hepes, 2.5 mM probenecid, 0.1% BSA (DMEM assay buffer) cells were loaded with 4 μM Fluo-4 in the same DMEM assay buffer for 2 h at 30 °C. Excess dye was removed and cells were washed with DMEM assay buffer. Compounds were added to the assay plate, and cells were monitored for 60 min with a FLIPR (488 nm excitation; 510–570 nm emission; Molecular Devices).

2.6. Electronic cell sensor technology and measurement of cell electrode impedance using the xCelligence system

The xCelligence system (Roche Diagnostics) is based on the ACEA RT-CES cell sensor electrodes which allow monitoring and analysis of the kinetic aspects of cellular behavior. The technology is described in detailed elsewhere [23]. Briefly, cell sensor array electrodes are integrated in the bottom of 96-well plates (E-plates) covering 80% of the surface area of the well. Impedance measured between electrodes in an individual well depends on electrode geometry, ionic concentration in the well, and whether there are cells attached to the electrodes. Cells attached to the electrode sensor surface will alter the local ionic environment at the electrode/solution interface, leading to an increase in the impedance. The more cells there are on the electrodes, the larger the increase in cell electrode impedance. Furthermore, the cell electrode impedance also depends on cell morphology and the extent to which cells attach to the electrodes.

To quantify cell status based on the measured cell electrode impedance, a parameter termed cell index (CI) is calculated [22] according to the formula:

$$\mathrm{CI} = \max\left(\frac{R_{\mathrm{cell}}(f)}{R_0(f)} - 1\right)$$

where $R_{\mathrm{cell}}(f)$ and $R_0(f)$ are frequency-dependent electrode resistance with or without cells present in the well, respectively. For these experiments a frequency of 10 kHz was chosen. Under the same physiological conditions, more cells attached on to the electrodes lead to a larger value for CI. For the same number of cells present in the well a change in the cell status such as cell spreading or cell adhesion will lead to a change in CI [23].

Data were analyzed using the xCelligence software package expressing changes in cell electrode impedance as changes in CI [25]. The kinetics shown represent average ± standard deviation for at least two measurements.

2.7. Determination of cell electrode impedance changes

Background impedance of E-plates (Roche Diagnostics) was determined prior to the addition of cells. Cells were added and incubated overnight to allow attachment. Medium was removed and 135 µl HBSS-20 mM HEPES (Gibco) was added. The cells were inserted in the xCelligence Station (Roche Diagnostics) and equilibrated for 45 min. For addition of compounds the E-plates were removed from the station, compounds were added with a Liquidator (Mettler Toledo, Switzerland) within 45 s. Plates were replaced in the station and impedance measurement was started using single frequency settings. Measurements were taken every 10 s for the first 15 min and every 60 s for the following 2 h. Thereafter measurements were taken every 5 min for 5 h and every 30 min for the following 10–15 h.

2.8. Materials

All compounds were obtained from Sigma, unless otherwise stated.

3. Results

3.1. Increasing intracellular Ca^{2+} concentration alters cellular impedance

The intracellular Ca^{2+} concentration in H295R cells can be increased either by releasing Ca^{2+} from intracellular stores by stimulation with AngII, which activates a G_q-coupled GPCR, or by stimulation with BayK8644 or FLP64176, which open voltage-dependent L-type Ca^{2+} channels. Changes in intracellular Ca^{2+} concentration were determined with the fluorescent Ca^{2+}-chelator Fluo-4. AngII induced a sharp transient increase in intracellular Ca^{2+} reaching a maximum within 60 s and decreasing to 40% of the maximum within further 30 s (Fig. 1A). In contrast opening of voltage-dependent L-type Ca^{2+} channels induces a slower increase in intracellular Ca^{2+} reaching a maximum after 3–5 min which is sustained at 80% of the maximum for 60 min (Fig. 1B–C). The maximal fluorescence signal observed in the presence of AngII was three times higher than the one observed with BayK8644 or FPL64176. The final plateau reached after AngII and BayK8644 stimulation was similar.

While AngII-induced increase and subsequent decrease in the fluorescence signal is a smooth curve, BayK8644 and FPL64176 show a wavelike response at intermediate concentrations with a frequency of 5 oscillations/100 s (1 µM BayK8644 and FPL64176, see insert). These wavelike responses are also visible at 10 and 3 µM in a single-well analysis (data not shown).

To analyze the time-dependent changes in Ca^{2+} concentration on a single cell level Ca^{2+}-imaging assays were performed (Fig. 2). Treatment with vehicle (top row) showed no visible change except for minor photobleaching compared to AngII (middle row) and BayK8644 (bottom row). Addition of AngII induced a Ca^{2+} response typical for a GPCR: a fast flash of (almost) all cells to a very bright intensity followed by a slower fading towards the original low intensity. Some cells blink individually after the initial concerted flash. In contrast, addition of BayK8644 produces bright concerted waves of Ca^{2+}-induced fluorescence that travel across the image plane. Groups of neighboring cells light up at $T = 0$ while others stay dark, then other groups at a different place light up while some go dark again (Fig. 2, circles). This is difficult to display in the image series and can be seen much better in the movies provided in the Supplementary Information.

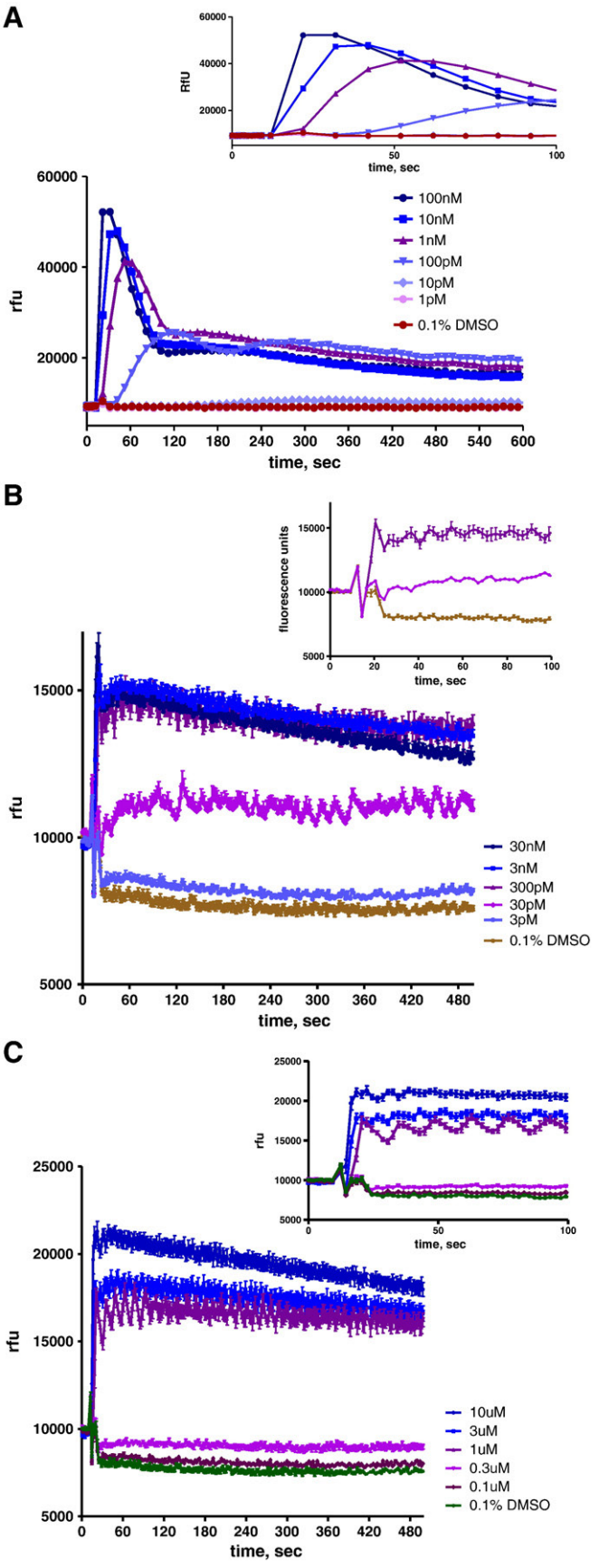

Fig. 1. Time-dependent changes in intracellular Ca^{2+} concentration after stimulation with angiotensin, BayK8644 and FLP64176. Cells were treated with increasing AngII (A), BayK8644 (B) or FLP64176 (C) at the indicated concentrations. (Data are shown as mean ± SD, $n = 6$). Intracellular Ca^{2+} concentration was monitored for 60 min. The graphs shows the first 10 min, the inserts the first 100 s. Data points were taken every 10 s (AngII) and every 2 s for BayK8644 and FLP64176.

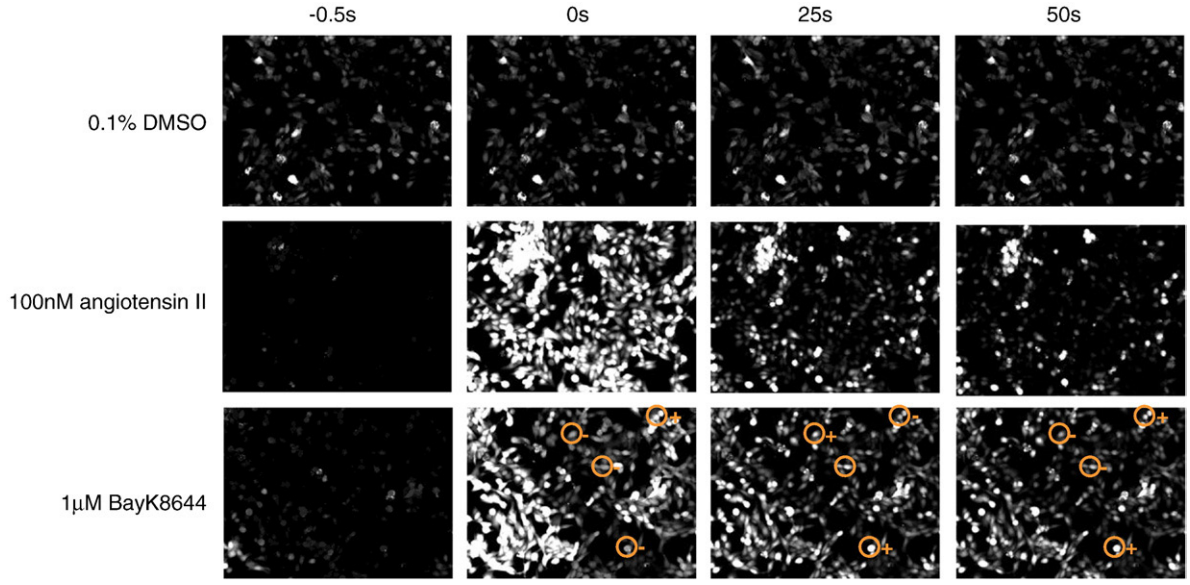

Fig. 2. Image series from fluorescent Fluo-4 [Ca^{2+}] time-lapse recordings of H295R adrenoma cells. Treatment with 0.1% DMSO (series 1, no visible change except for minor photobleaching) is compared to 100 nM AngII(series 2) and 1 μM BayK8644 (series 3).

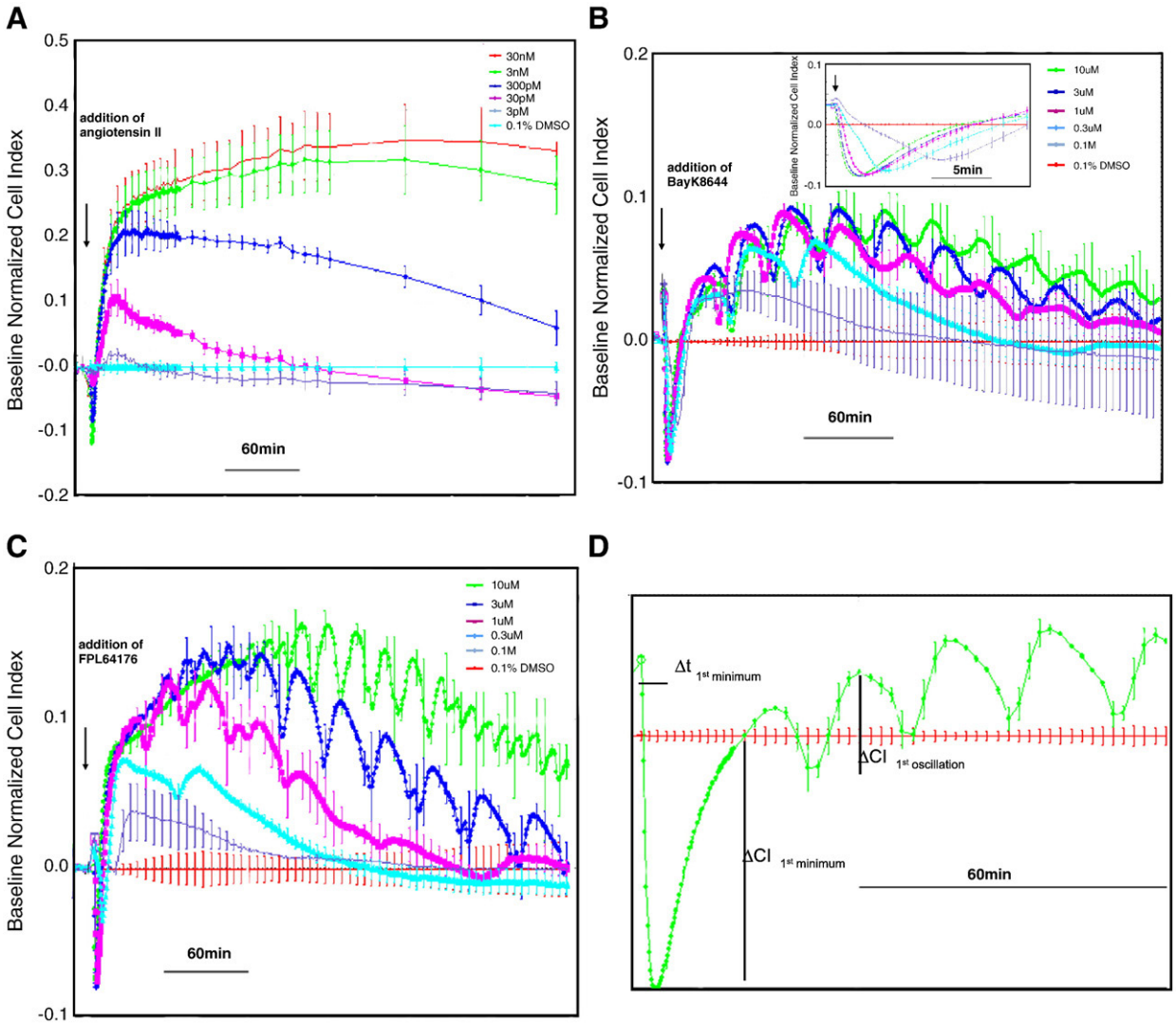

Fig. 3. Time-dependent changes in cellular impedance after stimulation with either AngII BayK8644 or FLP64176. Agonists were added 24 h after plating the cells and 60 min after changing the medium to buffer. (Data are shown as mean ± SD, $n = 6$). Cells were treated with AngII (A), BayK8644 (B) and FPL64176 (C). Concentrations used are indicated in the graph.

Changes in intracellular Ca^{2+} concentration have been shown to induce changes in cell morphology which can be detected with cellular impedance measurements [18,21,26]. We used this method to investigate possible morphological changes of cells for several hours after inducing an increase in intracellular Ca^{2+} concentration (Fig. 3). AngII induced a time-dependent change in cellular impedance typical for G_q-coupled receptor, i.e., a rapid dip followed by a slow, sustained increase in impedance (Fig. 3A). The observed EC_{50} of 0.12 ± 0.05 nM ($n = 3$) is comparable to the EC_{50} determined for AngII in other functional assays [27]. The time of maximal decrease and maximal increase in impedance stayed constant over the complete concentration range of AngII.

Similar to AngII, addition of BayK8644 or FPL64176 induced a rapid decrease in impedance. However, this was followed by several hours of impedance oscillations (Fig. 3B, C). In contrast to the effect observed with AngII, there is a concentration-dependent delay in the onset of oscillation (insert Fig. 3B). Three parameters of the oscillations were analyzed quantitatively: The time and amplitude of the first minimum, the amplitude of the first peak, the number of oscillations and their duration (Fig. 3D; Table 1). At 1 μM BayK8644 the onset of signal is delayed and duration of oscillations is reduced compared to 10 μM BayK8644, while signal size and frequency are similar. At 0.3 μM BayK8644 the onset is further delayed, signal size decreases and duration of oscillations is reduced. At 0.1 μM Bay8644 the immediate decrease in impedance is still occurring, while the oscillations are no longer induced.

To determine whether the oscillations induced by BayK8644 and FPL64176 are mediated by the opening of voltage-dependent Ca^{2+} channels, cells were treated with known Ca^{2+} channel inhibitors prior to the addition of BayK8644. Benedipine, a selective inhibitior of L-type Ca^{2+} channels [28,29], completely inhibited the oscillations induced by BayK8644 and FPL64176. However, there was no effect on the impedance changes induced by AngII (Fig. 4). Representatives of two chemical classes of L-type Ca^{2+} channels inhibitor: a phenylalkylamine (verapamil) and a benzothiazepine (diltiazem) did not prevent BayK8644-induced oscillations. However, from the dihydropyridines, benedipine, amlodipine and nifedipine were all effective. The most active inhibitor of induced oscillation was bendipine, completely inhibiting oscillations at 100 nM. Amlodipine ($IC_{50} = 2$ μM, $n = 2$) and nifedipine ($IC_{50} = 2.5$ μM, $n = 3$) were much less potent.

To identify the involvement of specific Ca^{2+} channel subunits a panel of siRNAs was applied 48 h prior to treatment with BayK8644. Of those siRNAs targeted to either alpha subtype or beta subtype only siRNA targeted to the α1d subunit inhibited oscillations (Fig. 5A). siRNA targeted to α1c, α1h, α2d1, α2d2, α2d3, β2, β3 subunits had no effect (data not shown). Suppression of subunit expression was assessed by qPCR (Fig. 5B). The results support that L-type Ca^{2+} channels are involved in the impedance oscillations.

3.2. Oscillations in impedance depend on regulation of intracellular Ca^{2+} concentration

Both releasing Ca^{2+} from intracellular stores by AngII or inducing Ca^{2+} influx across the plasma membrane by BayK8644 produced a rapid decrease of cellular impedance followed by a slower increase. In contrast to AngII, which produces an elevated and constant impedance signal, BayK8644 induced oscillations. We speculated that this might be caused by the oscillations in intracellular Ca^{2+}

Table 1
Quantification of BayK8644 induced oscillations: oscillations of six independent experiments were analyzed as indicated in Fig. 3D.

BayK8644	1st minimum		1st peak	Oscillations	
	Δimpedance, CI	Δtime, min	Δimpedance, CI	per hour	duration, h
10 μM	0.065 +/- 0.011	5.14 +/- 1.05	0.034 +/- 0.018	3.25 +/- 0.4	5.6 +/- 1.1
1 μM	0.07 +/- 0.010	5.75 +/- 1.03	0.038 +/- 0.015	3.3 +/- 0.8	3.2 +/- 0.8
0.3 μM	0.05 +/- 0.014	7.20 +/- 1.51	0.023 +/- 0.018	1.8 +/- 0.7	1.7 +/- 0.4

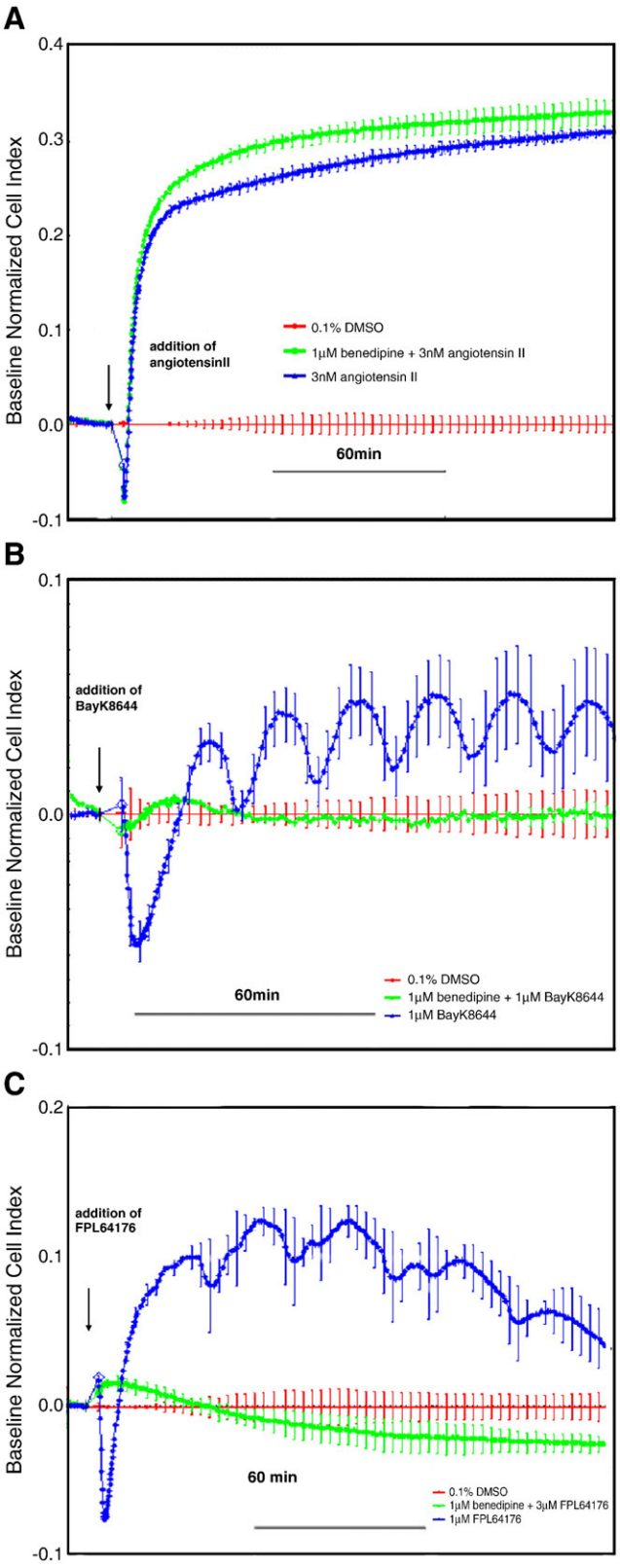

Fig. 4. Effect of benedipine on AngII, BayK8644 and FPL64177-induced changes in cellular impedance. Cells were pretreated with benedipine for 30 min prior to addition of AngII (A), BayK8644 (B), and FPL64176 (C). (Data are shown as mean ± SD, $n = 2$).

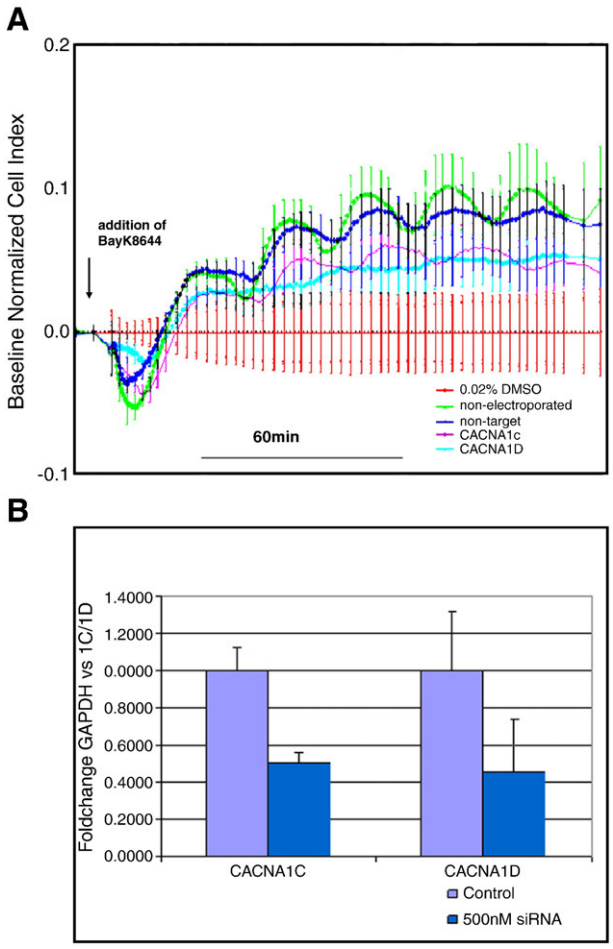

Fig. 5. Effect of siRNA directed to L-type Ca^{2+} channel subunits on BayK8644-induced oscillations in cellular impedance. Cells were electroporated with siRNA targeted to CACNA1C (α1c), CACNA1D (α1d), non-target siRNA, or non-electroporated (A). Each electroporation condition was corrected for its own baseline with 0.02% DMSO. 1 μM BayK8644 was added 48 h after electroporation. qPCR for CACNA1C and CACNA1D after 48 h treatment with the corresponding siRNA (B). (Data are shown as mean ± SD, $n = 2$).

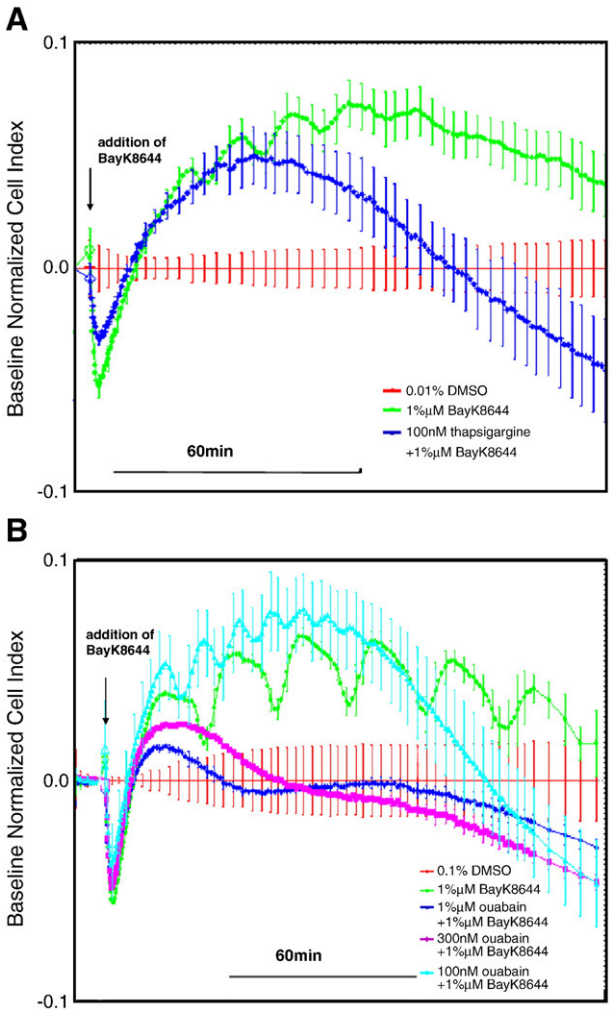

Fig. 6. Effect of thapsigargine and ouabain on BayK8644-induced oscillations in cellular impedance. Cells were treated for 30 min with 100 nM thapsigargine prior to addition of 1 μM BayK8644 (A). Cells were treated for 30 min with ouabain prior to addition of 1 μM BayK8644 (B) (Data are shown as mean ± SD, $n = 2$).

concentration, although these oscillations were much faster than those in impedance. Oscillations in intracellular Ca^{2+} concentration could be caused by two opposing mechanisms: extended Ca^{2+} influx through Ca^{2+} channels and uptake of Ca^{2+} into intracellular organelles or export of Ca^{2+} across the plasma membrane.

Therefore we investigated the mitochondrial Ca^{2+}-uniporter, the endoplasmic Ca^{2+}-transporter (SERCA) and the plasma membrane Na^+/Ca^{2+} exchanger. Thapsigargine, an inhibitor of SERCA, blocked BayK8644-induced oscillations completely, while the initial drop and subsequent increase in impedance were maintained (Fig. 6A). The shape of the curve is similar to the shape obtained after AngII addition (see Fig. 3A), which is caused by an increase in intracellular Ca^{2+} concentration. Ruthenium Red, an inhibitor of the mitochondrial Ca^{2+}-uniporter, had an effect similar to thapsigargine (data not shown).

To address, whether Ca^{2+} is also transported across the plasma membrane, ouabain, an inhibitor of the Na/K-ATPase to which the Na^+/Ca^{2+} exchanger is coupled, was used. The initial drop in signal was not inhibited, but oscillations were prevented. At lower concentrations, oscillations recovered, but with a smaller amplitude and higher frequency (Fig. 6B). These results support the hypothesis that the oscillations in cellular impedance are dependent not only on an increase in intracellular Ca^{2+} concentration but also on mechanisms that decrease the intracellular Ca^{2+} concentration.

3.3. Calmodulin mediates Ca^{2+}-dependent oscillations of impedance

Intracellular Ca^{2+} regulates many intracellular processes, including activation of protein kinase C and calmodulin-dependent kinases. Fig. 7 shows that inhibition of calmodulin with trifluoperazine reduced the amplitude of the initial drop in impedance (IC_{50} = 8.6 μM) and completely reduced oscillations at 10 μM (Fig. 7A). W7, a chemically unrelated calmodulin inhibitor had similar effects (data not shown). In contrast, inhibition of protein kinase C with the non-selective inhibitor GFX109203 did not prevent oscillations of impedance or the initial drop in impedance (data not shown).

One of the kinases regulated by calmodulin is myosin light chain kinase [13], which can be inhibited by ML-7. Pretreatment of cells with ML-7 prevented oscillations at 3 μM and reduced the amplitude of the oscillations even at 100 nM. The initial drop in impedance was reduced in a concentration-dependent manner with an $IC_{50} > 10$ μM (Fig. 7B).

Myosin light chain kinase and calmodulin have been shown to form a complex with nonmuscle myosin II, which has been shown to be associated with the F-actin network and to regulate exocytotic processes [15,18]. A specific inhibitor of myosin II ATPase activity, blebbistatin, was added to determine whether myosin II is the link between Ca and impedance changes (Fig. 8). The initial drop in

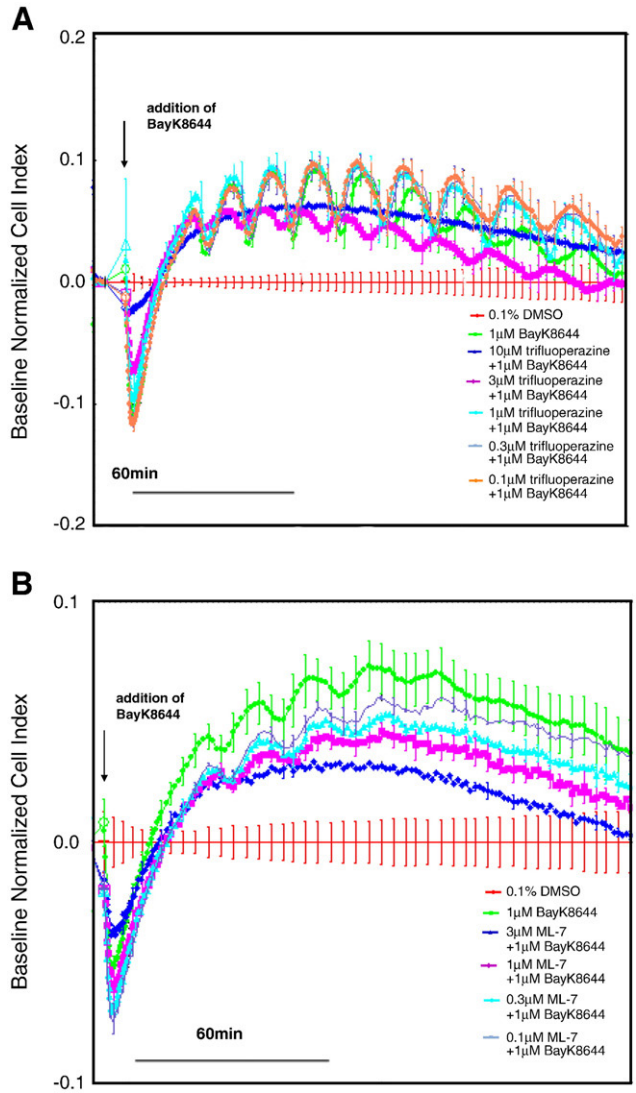

Fig. 7. Effect of calmodulin modulator treatment on BayK8644-induced oscillations in cellular impedance. Cells were treated for 30 min with trifluoperazine prior to addition of 1 μM BayK8644 (A). ML-7 was added to the cells 30 min prior to addition of 1 μM BayK8644 (B). (Data are shown as mean ± SD, $n = 2$).

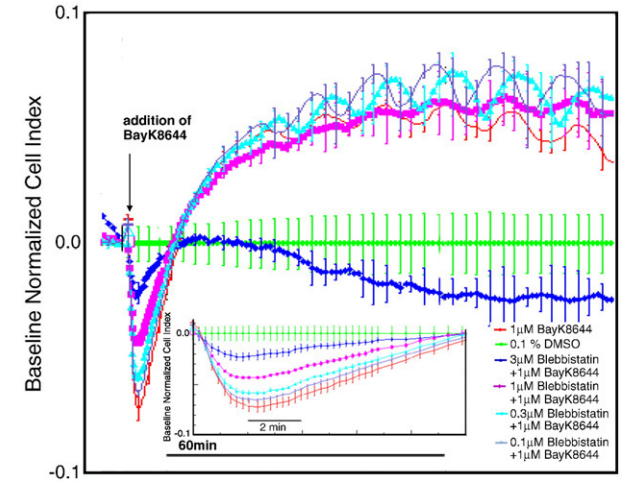

Fig. 8. Effect of blebbistatin treatment on BayK8644-induced oscillations in cellular impedance. Blebbistatin was added to the cells 30 min prior to addition of 1 μM BayK8644. (Data are shown as mean ± SD, $n = 2$).

impedance is reduced in a concentration-dependent manner with an IC_{50} of 1.8 μM (Fig. 8, insert). The subsequent oscillations are completely inhibited at 3 μM and recover at lower concentrations. Interestingly, at 300 nM oscillations are suppressed for about 60 min and then start with a lower amplitude.

Addition of latrunculin B, which depolymerizes actin filaments, induced a rapid massive decrease in impedance. No oscillations could be induced by BayK8644 after such pretreatment, indicating that polymerization of actin filaments is a prerequisite for oscillations of impedance (data not shown).

4. Discussion

Real-time cell electrical sensing (RT-CES) is a label-free technology that detects changes in the local ionic environment at the electrode/solution interface as increases or decreases in the electrode impedance. Such changes occur when cells interact with the electrode, for example due to an increase in cell number (proliferation) or due to gross morphological changes [25]. Using an instrument that can be placed in an incubator, cells can be kept under cell growth conditions. Thereby it is possible to continuously observe changes in impedance for several hours or even days [23,25,30]. The method was used to follow cell adhesion [23] as well as cell survival and toxicity [30]. In these experiments changes in impedance reflect increase or decrease of cell number or adherence of cells.

In addition to morphological changes on a prolonged timescale, it has been shown that stimulation of cell surface receptors induces rapid changes in cellular impedance due to slight alterations in cell morphology or cell adhesion. Thus, it has been demonstrated that activation of GPCRs [20,21] or tyrosine kinases [22] induced rapid changes in impedance that occurred within minutes. The observed impedance traces are specific for the type of receptor activated [21]. These results have been supported with another label-free technology based on optical dynamic mass redistribution, where GPCR activation [18] and interaction of ion channels with GPCR's [19] could be detected in real time. However, the question remains which cellular signaling pathways link the stimulation of the receptor to rapid changes in cellular morphology and adhesion which result in changes of cellular impedance. Early experiments had demonstrated that inhibition of actin polymerization with Latrunculin A, preventing polymerization of actin [31,32], is essential for cell adhesion and formation of cellular impedance [23]. Polymerization of actin is regulated by Ca^{2+}-dependent processes [33] suggesting that Ca^{2+} might be the second messenger linking receptor activation to cell morphology-related changes in impedance. Thus, any extracellular signal that alters the intracellular Ca^{2+} concentration could influence cellular impedance by changing the actin polymerization of the cell. Intracellular Ca^{2+} concentration can be elevated by activation of GPCRs, tyrosine kinases and opening of Ca^{2+} channels.

H295R cells express AngII receptors as well as L-type Ca^{2+} channels [34]. Activation of either results in an increase of intracellular Ca^{2+} concentration by activation of intracellular Ca^{2+} stores or influx of extracellular Ca^{2+}.

Ca^{2+} imaging assays demonstrated that AngII rapidly increased intracellular Ca^{2+}. This increase was not inhibited by benedipine, suggesting that Ca^{2+} originated from intracellular stores. Ca^{2+} mobiliziation was transient and rapidly decreased to a new plateau that was sustained for 60 min. In contrast opening of L-type Ca^{2+} channels rapidly increased intracellular Ca^{2+} concentration which was then sustained for 60 min. During the complete observation time, small oscillations in the Ca^{2+} concentration were observed indicating continuous process of Ca^{2+} influx and Ca^{2+} efflux from the cytoplasm. Similar results were observed with single cell imaging. AngII induced a rapid transient increase in the intracellular Ca^{2+} concentration, while BayK8644 induced a sustained increase with waves in the Ca^{2+} concentration that traveled back and forth across the image. These

distinct patterns of change in intracellular Ca^{2+} concentration resulted in two different patterns of time-dependent change in cellular impedance. While AngII induced a biphasic response resulting in a sustained increase in impedance, BayK8644 and FPL64176 induced an early drop in impedance followed by prolonged oscillations that lasted for several hours. Furthermore, the response to AngII was concentration dependent, however, the onset was independent of the concentration. In contrast, both size and onset of the response to BayK8644 were concentration dependent. Thus, although both AngII and BayK8644 increase intracellular Ca^{2+} concentration, the time course of impedance changes differ, suggesting that they are related to distinct signaling pathways [34].

Using selective inhibitors of the L-type Ca^{2+} channel and an siRNA for L-type Ca^{2+} channel subunit transfection we identified the α1d subunit of Ca_v1.3 as the plasma membrane target of BayK8644. Opening of Ca_v1.3 initiated the prolonged oscillations in impedance. The oscillations were also dependent on the activity of Ca^{2+} transport systems reducing intracellular Ca^{2+} concentration, ruthenium red sensitive mitochondrial Ca^{2+} uniporter [35] thapsigargine sensitive endoplasmic Ca^{2+}-ATPase [36] and ouabain-sensitive plasma membrane Na^+/Ca^{2+} exchanger [37]. However, influx from intracellular Ca^{2+} stores, which mediate AngII-induced signaling [11], was not involved in the BayK8644-induced oscillations (data not shown). Thus oscillations in impedance are caused by a tightly regulated intracellular Ca^{2+} concentration that is oscillating over a prolonged period of time in the presence of L-type Ca^{2+} channel openers.

Cellular targets of Ca^{2+} include protein kinase C and calmodulin-dependent kinases. While inhibiting protein kinase C did not prevent impedance oscillations, inhibition of calmodulin-dependent kinase reduced the impedance oscillations, indicating that BayK8644-induced oscillations are mediated by the calmodulin pathway. Targets of the calmodulin pathway include myosin II [13] and stress fiber formation [14] which link directly to cell morphology. Indeed, BayK8644-induced impedance oscillations are mediated by the nonmuscle myosin II, as shown by the inhibitor effect of blebbistatin, which selectively blocks myosin II [38]. Interestingly, nonmuscle myosin has not only been demonstrated to be involved in maintaining stress fiber integrity and basal cell tonus [12] but also to sustain an open exocytic fusion pore in secretory epithelial cells [16] and to regulate exocytosis in adrenal chromaffin cells [15]. Exocytosis increases the plasma membrane surface area, which is subsequently compensated by rapid endocytosis [4]. Such cycling in plasma membrane surface area could be the cause of the oscillations in cellular impedance observed during stimulation with BayK8644.

In summary, the present results suggest that opening L-type Ca^{2+} channels in human adrenocortical H295R cells induces sustained oscillations in cell electrode impedance via a calmodulin mediated pathway that involves actin polymerization. The prolonged activation of this pathway possibly results in induction of exocytosis that is accompanied by endocytosis to control the cell surface area. These cycles are stabilized over a prolonged period of time.

5. Conclusion

Intracellular Ca^{2+} concentration can be raised by several mechanism, activating Ca^{2+} either from intracellular stores or from extracellular space. The rise in Ca^{2+} concentration subsequently activates a number of cellular processes including morphological changes.

Here we demonstrate that activation of Ca^{2+} from intracellular stores and extracellular space showed discernible timecourse of the change in intracellular Ca^{2+} concentration and resulted in distinguishable morphological changes which could be continuously analyzed with label-free real-time impedance technology. Results obtained with inhibitors of the involved signaling pathways suggest that the changes in impedance are linked to exo/endocytosis cycling. This technology will make it feasible to investigate the link between cellular signaling and morphological changes of the cell for further receptors and ion channels.

Supplementary materials related to this article can be found online at doi: 10.1016/j.bbamcr.2011.01.016.

Acknowledgement

The authors would like to thank Sannah Zoffmann, Friedrich Metzger and Eric Niesor for valuable discussions and Jeremy Beauchamp for critically reading the manuscript.

References

[1] W.E. Rainey, I.M. Bird, J.I. Mason, The NCI-H295 cell line: a pluripotent model for human adrenocortical studies, Mol. Cell. Endocrinol. 100 (1994) 45–500.
[2] H.S. Willenberg, I. Ansurudeen, K. Schebesta, M. Haase, B. Wess, S. Schinner, A. Raffel, M. Schott, W.A. Scherbaum, The endothelium secretes interleukin-6 (IL-6) and induces IL-6 and aldosterone generation by adrenocortical cells, Exp Clin Endocrinol Diabetes 116 (2008) S70–S74.
[3] M. Szekeres, G.L. Nadasy, G. Turu, K. Supeki, L. Szidonya, L. Buday, T. Chaplin, A.J.L. Clark, L. Hunyady, Angiotensin II-induced expression of brain-derived neurotrophic factor in human and rat adrenocortical cells, Endocrinology 151 (2010) 1695–1703.
[4] H. von Grafenstein, C.S. Roberts, P.F. Baker, Kinetic analysis of the triggered exocytosis/endocytosis secretory cycle in cultured bovine adrenal medullary cells, J. Cell. Biol. 103 (1986) 2343–2352.
[5] N. Rouze, E. Schwartz, Continuous and transient vesicle cycling at a ribbon synapse, J. Neurosci. 18 (1998) 8614–8624.
[6] S.A. Chan, R. Chow, C. Smith, Calcium dependence of action potential-induced endocytosis in chromaffin cells, Pflugers Arch. - Eur. J. Physiol. 445 (2003) 540–546.
[7] A.E. Perez Bay, L.I. Ibanez, F.D. Marengo, Rapid recovery of releasable vesicles and formation of nonreleasable endosomes follow intense exocytosi in chromaffin cells, Am. J. Physiol. Cell. Physiol. 293 (2007) C1509–C1522.
[8] F. Van Goor, D. Zivadinovic, A.J. Martinez-Fuentes, S.S. Stojilkovic, Dependence of pituitary hormone secretion on the pattern of spontaneous voltage-gated calcium influx, J. Biol. Chem. 276 (2001) 33840–33846.
[9] J. Martins Rosa, A.M.G. de Diego, L. Gandia, A.G. Garcia, L-type calcium channels are preferentially coupled to endocytosis in bovine chromaffin cells, Biochem. Biophys. Res. Commun. 357 (2007) 834–839.
[10] E.A. Ertel, K.P. Campbell, M.M. Harpold, F. Hofmann, Y. Mori, E. Perez-Reyes, A. Schwartz, T.P. Snutch, T. Tanabe, L. Birnbaumer, R.W. Tsien, W.A. Catterall, Nomenclature of voltage-gated calcium channels, Neuron 25 (2000) 533–535.
[11] H. Qin, P. Kent, C.M. Isales, P.M. Parker, M.V. Wilson, W.B. Bollag, The role of calcium influx pathways in phospholipase D activation in bovine adrenal glomerulosa cells, J. Endocrinol. 202 (2009) 77–86.
[12] Z.M. Goeckeler, P.C. Bridgman, R.B. Wysolmerski, Nonmuscle myosin II is responsiblefor maintaining endothelial cell basal tone and stress fiber integrity, Am. J. Physiol. Cell. Physiol. 295 (2008) C994–C1006.
[13] F. Hong, B.D. Haldeman, O.A. John, P.D. Brewer, Y.-Y. Wu, S. Ni, D.P. Wilson, M.P. Walsh, J.E. Baker, C.R. Cremo, Characterization fo tightly associated smooth muscle myosin-myosin ligh chain kinase calmodulin complexes, J. Mol. Biol. 390 (2009) 879–892.
[14] J. Yuan, G.-X. Shi, Y. Shao, G. Dai, J.-N. WEi, D.C. Chang, C.-J. Li, Calmodulin bound to stress fibers but not microtubules involves regulation of cell morphology and motility, Int. J. Biochem. Cell. Biol. 40 (2008) 284–293.
[15] B.W. Doreian, T.G. Fulop, C.B. Smith, Myosin II activation and actin reorganization regulate the mode of quantal exocytosis in mouse adrenal chromaffin cells, J. Neurosci. 28 (2008) 4470–4478.
[16] P. Bhat, P. Thorn, Myosin 2 maintains an open exocytic fusion pore in secretory epithelial cells, Mol. Biol. Cell. Biol. 20 (2009) 1795–1803.
[17] W. Shin, K.D. Gillis, Measurement of changes in membrane surface morphology associated with exocytosis using scanning ion conductance microscopy, Biophys. J. 15 (2006) 262–265.
[18] A. Kebig, E. Kostenis, K. Mohr, M. Mohr-Andrae, An optical dynamic mass redistribution assay reveals biased signaling of dualsteric GPCR activators, J. Rec. Signal Transduction 29 (2009) 140–145.
[19] M. Fleming, L. Kaczmarek, Use of optical biosensors to detect modulation of slack potassium channels by G protein coupled receptors, J. Rec. Signal Transduction 29 (2009) 173–181.
[20] N. Yu, J.M. Atienza, J. Bernard, S. Blanc, J. Zhu, X. Wang, X. Xu, Y.A. Abassi, Real-time monitoring of morphological changes in living cells by electronic cell sensor arrays: an approach to study g protein-coupled receptors, Anal. Chem. 78 (2006) 35–43.
[21] M.F. Peters, C.W. Scott, Evaluating Cellular Impedance assays for detection of GPCR pleiotropic signalin and functional selectivity, J. Biomol. Screening 14 (2009) 246–255.
[22] J.M. Atienza, N. Yu, X. Wang, X. Xu, Y.A. Abassi, Label-free and real-time cell-based assay forscreening selective and potent receptor tyrosine kinase inhibitors using microelectronic sensor array, J. Biomol. Screening 11 (2006) 634–643.

[23] J.M. Atienza, L. Zhu, X. Wang, X. Xu, Y.A. Abassi, Dynamic monitoring of cell adhesion and spreading on microelectronic sensor arrays, J. Biomol. Screening 10 (2005) 795–805.
[24] D. Rampe, B. Anderson, V. Rapien-Pryor, T. Li, R.C. Dage, Comparison of the in vitro and in vivo cardiovascular effects of two structurally distinct Ca++ channel activators, BayK8644 and FPL64176, J. Pharmacol. Exp. Ther. 265 (1993) 1125–1130.
[25] J.Z. Xing, L. Zhu, J.O. Jacson, S. Gabos, X.-J. Sun, W.-B. Wang, X. Xu, Dynamic monitoring of cytotoxicity on microelectronic sensors, Chem. Res. Toxicol. 18 (2005) 114–161.
[26] J. Meshki, S.D. Douglas, J.-P. Lai, L. Schwartz, L.E. Kilpatrick, F. Tuluc, Neurokinin1 receptor mediates membrane blebbing in HEK293 cells through a rho/rho-associated coiled-coil kinase-dependent mechanism, J. Biol. Chem. 284 (2009) 9280–9289.
[27] H. Wei, S. Ahn, S.K. Shenoy, S.S. Karnik, L. Hunyady, L.M. Luttrell, R.J. Lefkowitz, Independent beta-arrestin 2 and G protein-mediated pathways for angiotensin II activation of extracellular signal-regulated kinases 1 and 2, Proc. Natl. Acad. Sci. U S A 100 (2003) 10782–10787.
[28] Y. Mori, G. Mikala, G. Varadi, T. Kobayashi, S. Koch, M. Wakamori, A. Schwartz, Molecular pharmacology of voltage-dependent calcium channels, Jpn. J. Pharmacol. 72 (1996) 83–109.
[29] A. Zharadnikova, I. Minarovic, I. Zharadnik, Competitive and cooperative effects of BayK8644 on the L-type calcium channel current inhibition by Clackum channel antagonists, J. Pharmacol. Exp. Ther. 322 (2007) 638–645.
[30] J. Glamann, A.J. Hansen, Dynamic detection of natural killer cell-mediated cytotoxidity and cell adhesion by electrical impedance measurements, Assay and Drug Development Technologies 4 (2006) 555–563.
[31] E. Zamir, M. Katz, Y. Posen, N. Erez, K.M. Yamda, B.Z. Katz, S. Lin, D.C. Lin, A. Bershadsky, Z. Kam, B. Geiger, Dynamics and segregation of cell matrix adhesions in cultured fibroblasts, Nature Cell Biology 2 (2000) 191–196.
[32] B. Wildt, D. Wirtz, P. Searson, Programmed subcellular release for studying the dynamics of cell detachment, Nature Methods 6 (2009) 211–213.
[33] U. Lindberg, C.E. Schutt, R.D. Goldman, M. Nyakern-Meazza, L. Hillberg, L.S. Rathje, S. Grenklo, Tropomyosins regulate the impact of actin binding proteins on actin filaments, Adv. Exp. Med. Biol. 644 (2008) 223–231.
[34] R.G. Clerc, A. STauffer, F. Weibel, E. Hainaut, A. Perez, J.-C. Hoflack, A. Benardeau, P. Pflieger, J.M.R. Garriz, J.W. Funder, A.M. Capponi, E.J. Niesor, Mechanisms underlying off-target effects of the cholesteryl ester transfer protein inhibitor torcetrapib involve L-type calcium channels, Hypertension 28 (2010) 1676–1686.
[35] C.S. Rossie, F.D. Vasington, E. Carafoli, The effect of ruthenium red on the uptake and rlease of Ca2+ by mitochondria, Biochem. Biophys. Res. Commun. 50 (1973) 846–852.
[36] G. Inesi, S. Hua, C. Xu, H. Ma, M. Seth, A.M. Prasad, C. Sumbilla, Studies of Ca2+ ATPase (SERCA) inhibition, J. Bioenerg. Biomembr. 37 (2005) 365–368.
[37] A.A. McDonough, J.B. Velotta, R.H. Schwinger, K.D. Philipson, R.S. Farley, The cardiac sodium pump: structure and function, Basic. Res. Cardiol. 97 (2002) 19–24.
[38] M. Kovacs, J. Toth, C. Hetenyi, A. MaInasi-Csizmadia, J.R. Sellers, Mechanism of blebbistatin inhibition of myosin II, J. Biol. Chem. 279 (2004) 35557–35563.